Modeling the thickness dependence of the magnetic phase transition temperature in thin FeRh films

Thomas Andrew Ostler,[1,2,*] Craig Barton,[3] Thomas Thomson,[3] and Gino Hrkac[2,4]

[1]*Université de Liège, Physique des Matériaux et Nanostructures, Liège, B-4000 Sart Tilman, Belgium*
[2]*College of Engineering, Mathematics and Physical Sciences, The University of Exeter, Exeter EX4 4SB, United Kingdom*
[3]*School of Computer Science, The University of Manchester, Oxford Road, Manchester M13 9PL, United Kingdom*
[4]*Institute for Analysis and Scientific Computing, TU Wien, Vienna, Austria*

FeRh and its first-order phase transition can open new routes for magnetic hybrid materials and devices under the assumption that it can be exploited in ultra-thin-film structures. Motivated by experimental measurements showing an unexpected increase in the phase transition temperature with decreasing thickness of FeRh on top of MgO, we develop a computational model to investigate strain effects of FeRh in such magnetic structures. Our theoretical results show that the presence of the MgO interface results in a strain that changes the magnetic configuration which drives the anomalous behavior.

I. INTRODUCTION

Iron rhodium is an example of a magnetic material that undergoes a change in its magnetic order from antiferromagnetic to ferromagnetic. Discovered almost 80 years ago [1], the origin of this unusual first-order metamagnetic phase transition is still debated [2–5]. In bulk alloys with atomically equal amounts of iron and rhodium the crystal structure is a $B2$ (CsCl-type) structure and changes from an antiferromagnet at low temperatures to a ferromagnet as the temperature is increased to around 50–60 K above room temperature. At that same point the lattice also undergoes a volume expansion [4]. There has been much debate as to whether this phase transition is driven by structural effects, such as lattice expansion, or purely magnetic interactions [6], such as magnetovolume effects or a superposition of the two [7]. In Ref. [5] it was shown that ultrashort laser pulses were able to drive the magnetic phase transition and concluded that the phase transition was accompanied, but not driven, by a lattice expansion. In contradiction to this, Mariager and co-workers [4] showed that the two occurred simultaneously, which has been supported by other theoretical works [7].

Previous studies have shown that it is possible to tune the temperature at which this transition occurs by, for example, varying the composition of iron or rhodium [8], doping with other elements [2,8,9], such as Pd, Pt, or Ir, or straining the sample [10]. Excitation of the phase transition occurs when energy is added to the system allowing one to use a wide range of stimuli to induce the metamagnetic phase transition, such as, electric field [11], temperature [1], applied magnetic fields [12,13], pressure [14], and spin-polarized currents [15] making it a tempting candidate for future magnetic-based technological devices.

Due to the flexibility in controlling this phase transition, FeRh is undergoing renewed interest [9,16–18] for the development of new devices, such as for low-energy electric-field controlled magnetic recording as an alternative to heat assisted magnetic recording [19], or as a magnetic switch using an exchange-coupled composite [8,20]. For such applications,

interfacing FeRh with other materials, such as ferromagnets [8] or ferroelectrics [19], is required to functionalize the phase transition. Potential applications are reinforced by very recent work demonstrating control of the phase transition of thick FeRh films in an artificial multiferroic [21]. However, realizing devices based on FeRh, for example, in magnetic storage will inevitably require thicknesses of the layers below 10 nm. This can pave the way to high magnetic densities and enable enhanced functionality in even smaller devices. In such applications the ability to simultaneously preserve and move the phase transition presents another significant challenge.

In 2013, Han *et al.* [22] demonstrated the thickness dependence of the phase transition temperature in FeRh deposited on Si/SiO wafers with a MgO buffer layer. They showed that as the thickness of FeRh in those samples decreased the phase transition temperature also decreased. In the present paper we show an opposite trend occurs in FeRh deposited on single-crystal MgO [23]. Motivated by the need to understand the origin of these seemingly contradictory findings we have developed a model to try to understand this shift based on an assumed strain effect arising from the interface that modifies the underlying magnetic exchange interactions.

II. EXPERIMENTAL SETUP AND RESULTS

We begin by describing the experimental results where a series of $Fe_{50}Rh_{50}$ thin films ranging from 2.5 to 10 nm were dc magnetron sputtered onto (001) MgO substrates [24]. The substrate preparation involved cleaning the MgO in isopropyl alcohol using an ultrasonic bath. The depositions were performed using a target power of 100 W from a 50:50 FeRh target and a working pressure of 3 mTorr. The substrate temperature during the deposition was 650 °C which was increased to 750 °C following deposition of the film to postanneal the FeRh.

The temperature-dependent magnetization of the set of samples was measured using vibrating sample magnetometry (VSM) using a Microsense Model 10 vector VSM in the range of 300–475 K. These measurements where performed using an in-plane applied magnetic field of 1 kOe to ensure alignment and saturation of the magnetic domain structure in addition to a 50-point sampling average. The samples were
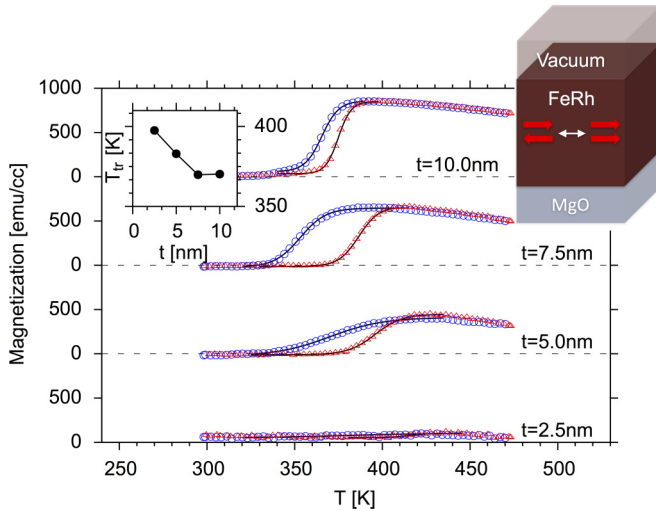
*thomas.ostler@ulg.ac.be

FIG. 1. Experimentally determined magnetization as a function of temperature during heating (red triangular points) and cooling (blue circular points). The black curves are fits to the data in the region of the transition, and the data has been offset for clarity. The left inset shows the extracted transition temperature as a function of thickness using the procedure described in the text. The schematic inset on the right shows diagrammaticality the FeRh/MgO structure.

cut using a Southbay disk cutter to create an 8-mm disk for the VSM measurement. The diamagnetic contribution of the 8-mm MgO substrate disk (plus quartz holder) was measured using the same measurement conditions described previously and directly subtracted from the raw VSM data. This was then smoothed using a 10-point Savitzky-Golay digital filter to aid data analysis (points in Fig. 1). To determine the phase transition temperature, we use a curve fitting procedure in the region of the phase transition (lines in Fig. 1). The fitting function we have used is as follows:

$$m(T) = a \, \tanh\left(\frac{T - T_{tr}}{\Delta T}\right) + b, \tag{1}$$

where T_{tr} is the transition temperature, ΔT is a measure of the slope of the transition, a is a measure of the saturation magnetization change, and b is an arbitrary offset which is close to zero. The phase transition temperature is then taken as the midpoint between T_{tr} in the heating and the cooling case.

A schematic of the structure of the FeRh/MgO bilayer is shown in Fig. 1. The magnetization values were taken at 1 kOe as a function of temperature and are shown for different thicknesses of FeRh. From the data it can be seen that as the film thickness is reduced, an increase in the transition temperature is seen. This is shown explicitly in the left hand inset of Fig. 1. The curve shows an almost linear decrease initially with little change between the 7.5- and the 10-nm samples as the film thickness is increased. In comparison to that of the work by Han *et al.* [22] the trend is reversed. Our aim is to attempt to understand if this increase in the phase transition temperature can be explained by the difference between the two substrates (Si/SiO/MgO buffer and MgO, respectively) rather than arising from the reduction in the thickness of FeRh itself, for example, due to loss of coordination at the surface.

We therefore developed a numerical model of the interface system which is outlined below.

A. Numerical model

There are a number of theoretical/computational models that can describe the ferromagnetic (FM) or antiferromagnetic (AFM) phase [25–28] and first-principles models can be used to understand the effects of interfaces and atomic termination [29]. The present approach allows for the simultaneous description of both the FM and the AFM phases using a single set of parameters, based on the atomistic spin dynamics formalism [30]. This second-principles model is based on a Heisenberg Hamiltonian as presented by Barker and Chantrell [6]. They showed that it is possible to reproduce the phase transition through the contribution of exchange terms, which implies a magnetic origin of the phase transition [3]. Such nonlinear terms were assumed to be important in explaining the nonlinear variation of the induced magnetic moment on rhodium arising from the Weiss field of Fe [31]. The Hamiltonian contains contributions from bilinear and four-spin exchange interactions,

$$\mathcal{H} = -\sum_{i,j} J_{ij}(\mathbf{S}_i \cdot \mathbf{S}_j) + \sum_{i,j,k,l} D_{ijkl}(\mathbf{S}_i \cdot \mathbf{S}_j)(\mathbf{S}_k \cdot \mathbf{S}_l). \tag{2}$$

Here J_{ij} and D_{ijkl} are the bilinear and four-spin terms, respectively, that take the values given in Ref. [6]. As was shown in Ref. [6], the four-spin term has a different temperature scaling from the bilinear term which gives rise to a competition between ferromagnetic (bilinear) and antiferromagnetic (four-spin) order. The dynamics of each spin in the system $\mathbf{S}_i$ are calculated by integrating the stochastic Landau-Lifshitz-Gilbert (LLG) [32–34] equation,

$$\dot{\mathbf{S}} = -\frac{\gamma_i}{(1 + \lambda_i^2)\mu_i}\mathbf{S}_i \times [\mathbf{H}_i + \lambda_i \mathbf{S}_i \times \mathbf{H}_i], \tag{3}$$

where the fields are given by

$$\mathbf{H}_i = -\frac{\partial \mathcal{H}}{\partial \mathbf{S}_i} + \boldsymbol{\xi}_i, \tag{4}$$

and γ_i is the gyromagnetic ratio, λ_i is the coupling to the thermal bath, μ_i is the atomic magnetic moment, and $\boldsymbol{\xi}_i$, a fluctuating stochastic term, which has zero mean and a variance given by $\langle \xi_i^\alpha(t)\xi_j^\beta(t') \rangle = 2\lambda_i k_B T \mu_i \delta_{ij}\delta_{\alpha\beta}\delta(t - t')/\gamma_i$. The use of the white-noise correlator in the present paper is justified on the grounds that we are considering equilibrium quantities and the effect of electronic correlations are negligible. In the Hamiltonian (1) an adiabatic approximation is made such that the rhodium moment is assumed to appear due to the Weiss field from iron on a much faster time scale than the precession of the magnetic moments. To that end, the Hamiltonian is written in terms of the Fe degrees of freedom only [6]. The four-spin term in the Hamiltonian that arises due to electron hopping among four sites must be calculated taking into account all of the 32 (nearest-neighbor quartets) [35]. The anisotropy constant K_i we take from Ref. [36], although we include only the largest term which was shown to be at least two orders of magnitude larger than the other anisotropy constants that were measured. We note that, in Ref. [29], it was shown that for very thin FeRh films (2 to 3nm) there was a much

larger anisotropy value although not for FeRh on MgO. In our modeling we have neglected this large anisotropy value for the thinnest samples so that we could understand the effects of exchange only on the transition temperature. The constants used in Eq. (1) and the LLG equation [Eq. (3)] are given in Table I. The Zeeman field **B** takes a small value of 0.05 T in the x direction so that there is a predefined orientation for the spins.

We solve the LLG equation of motion using the Heun numerical scheme with a time step of 0.1 fs to ensure numerical stability. The in-plane system size is 48×48 unit cells, just under $15 \times 15 \, \text{nm}^2$ with periodic boundary conditions in the x and y (in-plane) directions. Although the calculation of the bilinear exchange can be calculated straightforwardly using Fourier-based methods, the more computationally expensive four-spin term cannot. Thus to allow us to numerically calculate the thermal hysteresis curves within a reasonable time we choose this in-plane system size.

As shown in the right hand schematic inset of Fig. 1, FeRh was deposited on MgO and whereas there is a reasonable match between FeRh orientated along the (110) directions and MgO along the (100) directions, there will inevitably be some strain at the interface due to lattice mismatch which will lead to a change in the electronic structure of the two materials. The effects of strain have been shown to be significant in FeRh [37]. In the following we have assumed that the strain induced in FeRh gives rise to a change in the exchange interactions due to the modification of the atomic positions and the electronic structure. The aim therefore was to vary systematically the exchange in the first few (here we assume five) planes immediately adjacent to the interface with MgO to see if: (i) the phase transition in FeRh is preserved, and (ii) how the exchange effects the transition temperature and how this compares with the present (and previous) experimental results. A schematic of the configurations used in the numerical model are shown in panel (a) of Fig. 2.

Here we report a systematic study of the effects of FeRh film thickness with and without the presence of a strained FeRh layer. We show that by changing the magnetic order of the strained layers (J_m) and between the strained and unstrained

FeRh (J_int) the transition temperature can be tuned over a range of values. Panels (b) and (c) of Fig. 2 show the different possible configurations due to varying the exchange in the strained layer. We restrict ourselves to the $B2$ structure and a G-type antiferromagnetic structure in both FeRh systems to restrict the possible phase space.

B. Thickness dependence—two-dimensional film

In the first instance we have calculated thermal hysteresis loops for a range of isolated FeRh films with vacuum on both sides without the presence of strain (arising from the MgO interface). In practical terms this is achieved in the simulation by having periodic boundary conditions in the plane and having a vacuum region out of the plane (above and below). Figure 3 shows the thermal hysteresis loops for a range of sample thicknesses where each data set is again offset for clarity. The thermal hysteresis loops are calculated by performing a heating and cooling simulation. First, starting at very high temperatures the temperature is lowered at a continuous rate of 500 K/ns until a temperature of at least 50 K above the transition temperature and then the rate is dropped to 50 K/ns until the phase transition is complete and then the lower temperatures are calculated at the 500 K/ns rate. Such rates are much faster than those normally used in magnetometry measurements. To qualitatively compensate for this discrepancy in our simulations we use a value of the coupling to the thermal bath $\lambda_i = 1.0$, which is much larger than measured experimentally [36] but somewhat accounts for the difference in time scales. For the heating case the opposite procedure is used, starting with the system in a G-type antiferromagnetic structure.

Clearly for thin films of FeRh there is a consistent decrease in the temperature at which the phase transition occurs as a function of thickness (shown explicitly in the inset of Fig. 3). This can be understood as follows: In an infinite bulk three-dimensional FeRh sample, the exchange interactions for each spin, both bilinear and four-spin, would be completely satisfied in all directions (there would be no free dangling exchange bonds, see the left-hand insets of Fig. 4). In our case, there are 18 (6 nearest- and 12 next-nearest) neighbors.

TABLE I. Parameters entering into the Heisenberg Hamiltonian and Landau-Lifshitz-Gilbert equations.

| Quantity	Symbol	Value	Units
FeRh nearest-neighbor bilinear exchange energy	J_{ij}	0.4×10^{-21}	(J)
FeRh next-nearest-neighbor bilinear exchange energy	J_{ij}	2.75×10^{-21}	(J)
FeRh four-spin exchange energy	$\boldsymbol{D}_{ij}$	0.23×10^{-21}	(J)
FeRh—interface material exchange	J_int	Varied	
Interface material nearest-neighbor exchange (bulk region)	J_m	Varied	
FeRh anisotropy energy	K_FeRh	-1.404×10^{-23}	(J)
FeRh gyromagnetic ratio	γ_FeRh	1.024	(γ_e)
FeRh magnetic moment	μ_FeRh	3.15	(μ_B)
FeRh thermal bath coupling constant	λ_FeRh	1.0	
Strained FeRh anisotropy energy	K_m	-1.404×10^{-23}	(J)
Strained FeRh gyromagnetic ratio	γ_m	1.024	(γ_e)
Strained FeRh magnetic moment	μ_m	3.15	(μ_B)
Strained FeRh thermal bath coupling constant	λ_m	1.0	
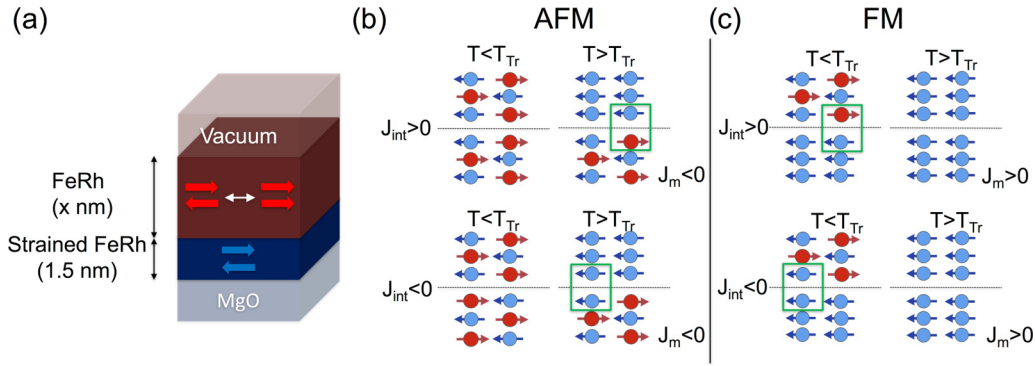
FIG. 2. (a) Schematic of the system configuration used in the numerical simulations. The top (dark red) layer is FeRh of varying thickness (x) and the bottom (dark blue) is the region of strained FeRh of thickness 1.5 nm and can be either antiferromagnetic ($J_m < 0$) as depicted here or ferromagnetic ($J_m > 0$), not shown. Depending on the exchange within the strained layer (J_m) and the exchange at the interface (J_{int}) with the unstrained FeRh there are four possible configurations of the spins as depicted in (b) AFM and (c) FM. Depending on the combination of J_m and J_{int}, either above or below the phase transition, there is always some frustration (green rectangles) where the exchange cannot be satisfied exactly. Note that the four-spin exchange is not included in the interface layer.

In the case of a two-dimensional film, at the surface the atoms cannot satisfy all bilinear or four-spin interactions. The bilinear term will still have full coordination within the plane, although it will only have half coordination perpendicular to the surface plane, therefore it will have five unsatisfied exchange interactions (one nearest neighbor and four next-nearest neighbors), shown schematically in the upper right panel of Fig. 4.

In the case of the four-spin term the lack of coordination has a much larger impact. For the four-spin term the central atom i in the bulk has 32 quartets, whereas at the interface it has half that number due to the ways of permuting over the four basic quartets [35].

As the in-plane dimensions of the calculated systems are fixed, one may expect a linear scaling of the phase transition temperature with thickness as the number of missing exchange interactions remains constant, therefore the surface-area-to-volume ratio decreases linearly. However, the scaling of the phase transition temperature with thickness as shown in the inset of Fig. 3 is nonlinear. This arises due to the fact that the bilinear and four-spin terms have a different temperature dependence [5].

Using the model that we have outlined we now extend the study to include a strained layer of FeRh. The thickness of the total amount of FeRh (including the strained layer) is varied as in Fig. 3, however, the amount of strained
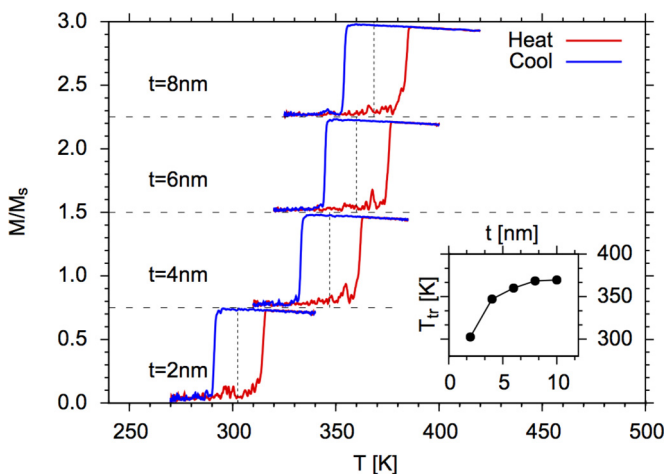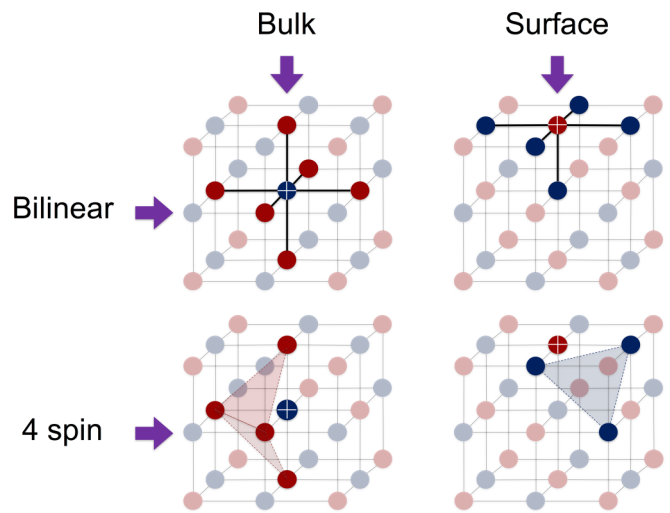

FIG. 4. Schematic of the difference between the bulk (left-hand side) and the surface (right-hand side) exchange interactions for the bilinear (upper row) and four-spin (lower row) terms. For the bilinear terms there are fewer dangling exchange bonds as the surface (in-plane) interactions are still included (for the nearest neighbors six interactions in bulk and five at the surface). However, for the four-spin terms there are half the number of complete quartets as the central atom (denoted with a white cross) must always interact with three spins from the other (antiferromagnetic) sublattice in the formation of one of the basic four quartets. Therefore, a fully coordinated atom in the bulk has 32 quartets (not all shown) and at the surface has just 16.

FIG. 3. Calculated thermal hysteresis curves for a range of FeRh thicknesses from 2 nm (lower) to 8 mn (upper) with the red lines representing the heating curve and the blue lines representing the cooling curve. The inset shows the transition temperature as a function of film thickness (taken as the midpoint between the cooling and the heating curves and found by fitting the data as discussed in the text).
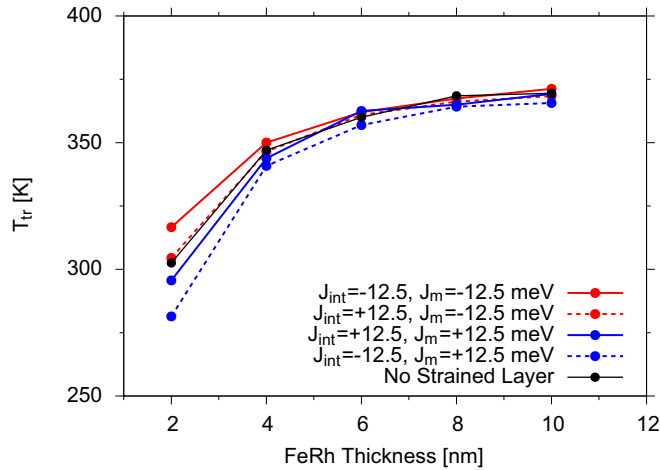
FIG. 5. Numerically determined transition temperatures as a function of FeRh thickness for a 1.5-nm strained FeRh layer. The red curves show the case for an antiferromagnetic interface material ($J_m < 0$), which both show an increase in the transition temperature, although the effect is reduced for a ferromagnetic interface coupling (J_{int}). For a ferromagnetic interface material ($J_m > 0$), the transition temperature is reduced, although the change is small for a ferromagnetic interface coupling ($J_{int} > 0$).

FeRh is fixed as shown in the schematic Fig. 2(a). We vary the exchange between the FeRh and the strained layers J_{int} and within the strained layer itself J_m, giving rise to four possible configurations for the magnetic structure. This is depicted for an antiferromagnetic strained layer Fig. 2(b) and a ferromagnetic one Fig. 2(c). Interestingly, depending on the combination of J_{int} and J_m, there is always an uncompensated (frustrated) interface as shown schematically by the green rectangles in Figs. 2(b) and 2(c). This frustration can be above or below the phase transition temperature as depicted. It has been shown previously that depending on the thickness of FeRh and whether the termination at the interface is an Fe or Rh atom the interface magnetism can change from G-type AFM (for the Fe termination) to FM (for the Rh termination) [29].

C. Ultrathin interface—effect of sign of interface and bulk exchange

Due to the spin pairing at the interface, the effect of the interface exchange plays a significant role in modifying the phase transition temperature. This is shown in Fig. 5 whereby a relatively small magnitude of the exchange ($|J_{int}|$ and $|J_m|$) is used in the strained layer (12.5 meV) and the signs of each of J_{int} and J_m are varied.

From Fig. 5 we see that by including a strained layer, depending on the balance between the interface (J_{int}) and the bulk exchange of the strained layer (J_m), a change in the transition temperature is observed. For an antiferromagnetic interface layer ($J_m < 0$), there is a consistent increase in the phase transition temperature, particularly below 6 nm of FeRh. As mentioned above, this is the consequence of uncompensated (frustrated) spins. The antiferromagnetic interface for both an antiferromagnetic and a ferromagnetic material gives the

largest change in the phase transition temperature (with respect to the system with no interface, black curve).

A negative value of J_m produces a strained layer with an antiferromagnetic structure which favors the antiferromagnetic (low-temperature) ground state and gives a higher transition temperature (T_{tr}) than the case of positive J_m, which favors a ferromagnetic ground state, i.e., the high-temperature phase pushes the transition temperature to lower values. For 8- and 10-nm FeRh thicknesses the transition temperatures are close to those for the case without an interface as the system becomes dominated by the FeRh layer. As the thickness is decreased the interface coupling becomes more important and starts to dominate, which makes growing thin-film structures with a perfect interface very challenging.

D. Ultrathin interface—effect of the strength of the bulk exchange value

So far we have shown the dependence of the phase transition temperature for different configurations of the strained layer. The value of the exchange used was a relatively low value, around 20% that of bulk bcc iron. For the antiferromagnetic strained layer configuration, increasing the exchange J_m might be expected to increase frustration, resulting in a reduced transition temperature. However, as we show in Fig. 6 for a 6-nm film, the phase transition temperature shows a clear increase. This is due to the fact that the antiferromagnetic order in the interface layer supports the four-spin terms as discussed above. For the ferromagnetic strained layer ($J_m > 0$), the trend is the opposite as the exchange supports ferromagnetic order in the FeRh layer. There is also an increasing magnetization below the phase transition temperature as the interface material imposes interface ferromagnetism with a larger correlation length with increasing exchange.

Thus far, decreasing the FeRh thickness has led to a reduction in the transition temperature. We initially assumed a low value of the exchange in the strained layer, and the question now arises, how does the transition temperature vary with thickness for different values of the exchange? Therefore, we performed simulations increasing the size of the exchange value in the strained region from -12.5 meV to a value of -28.1 meV as presented in Fig. 7. The exchange within the strained layer is equal to that at the interface with unstrained FeRh($J_m = J_{int}$), which are both negative. We observe that by increasing the exchange we see a recovery of the transition temperature up to the bulk FeRh phase transition value (dashed curve in Fig. 7). By further increasing the exchange, which is not unrealistic as a value of 28.1 meV corresponds to the Curie temperature of a nickel-based alloy, we see a further increase in the phase transition temperature. In the present paper, we have not investigated the effect of the thickness in the strained FeRh layer. We have, however, tested a strained FeRh layer of 3 nm and find that the results (not shown) are the same as those as in the 1.5-nm case. Further increases in this thickness would not represent interface strain, and the focus of the present paper was on the effects of ultrathin films with interface strain. As the results for the thickest films show, if one has a larger amount of material (i.e., a thicker film), the bulk regions begin to dominate the magnetic state.
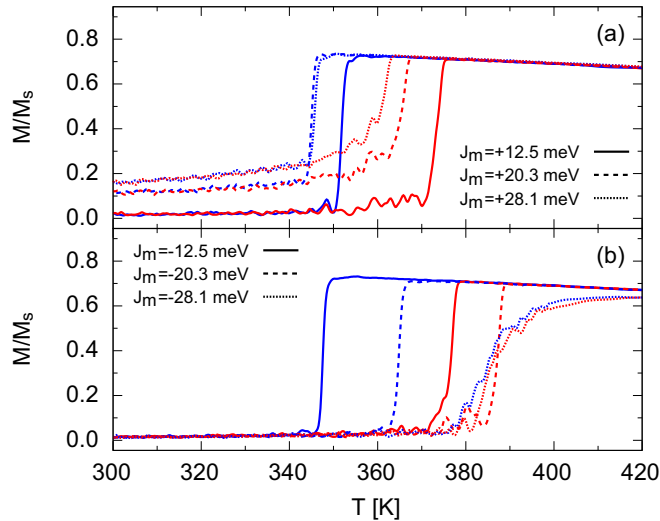
FIG. 6. Simulated thermal hysteresis curves (blue curve for cooling and red curve for heating) for a 6-nm FeRh layer and both (a) ferromagnetic and (b) antiferromagnetic strained layers for a range of exchange values of $|J_m|$ and $|J_{int}|$. The ferromagnetic interface shows a decreasing transition temperature with increasing exchange, whereas the antiferromagnetic is increasing.

III. DISCUSSION

By constructing a numerical model of ultrathin FeRh layers subject to possible strain at an interface with MgO we have shown that, depending on how the presence of the interface modifies the exchange interaction, the phase transition temperature as a function of film thickness can vary significantly. The exchange interaction in the strained layer plays an important role in determining the phase transition temperature, depending on whether it supports antiferromagnetic or ferromagnetic interactions. The results suggest that, depending on the choice of substrate, it is possible to tune the phase transition temperature. Furthermore, the general trends can be used to interpret experimental measurements. The numerical results are in good agreement with the results
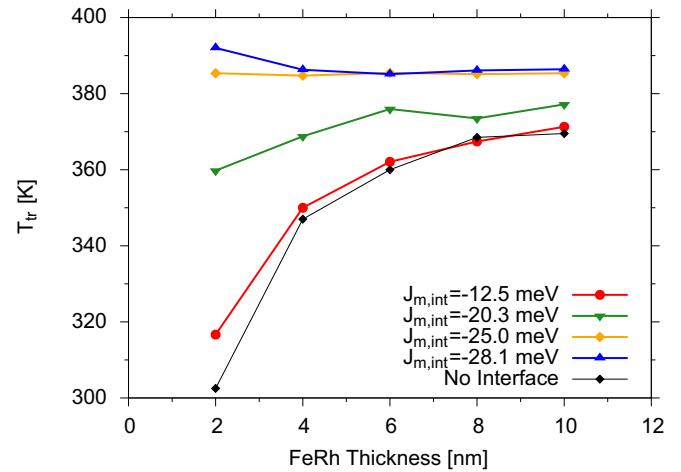

FIG. 7. Calculated transition temperature for a range of FeRh thicknesses for an antiferromagnetic strained FeRh layer ($J_m < 0$ and $J_{int} < 0$) for a range of exchange J_m and $J_{int}(J_m = J_{int})$. For low exchange in the strained layer (e.g., the red curve) there is an increasing transition temperature with thickness. The trend is reversed as the exchange is increased in the interface layer (the blue curve).

of a series of experimental samples showing a similar trend of increasing transition temperature with decreasing thickness. Importantly we have shown that the effect of interface effects become increasingly important for FeRh as one tries to engineer ultrathin films, particularly for functional devices based on FeRh [17,21,38].

ACKNOWLEDGMENTS

[1] M. Fallot and R. Hocart, Sur l'apparition du ferromagnétisme par élévation de température dans alliages de fer et de rhodium, Rev. Sci. **77**, 498 (1939).

[2] J. S. Kouvel, Unusual nature of the abrupt magnetic transition in FeRh and its pseudobinary variants, J. Appl. Phys. **37**, 1257 (1966).

[3] R. Y. Gu and V. P. Antropov, Dominance of the spin-wave contribution to the magnetic phase transition in FeRh, Phys. Rev. B **72**, 012403 (2005).

[4] S. O. Mariager *et al.*, Structural and Magnetic Dynamics of a Laser Induced Phase Transition in FeRh, Phys. Rev. Lett. **108**, 087201 (2012).

[5] G. Ju *et al.*, Ultrafast Generation of Ferromagnetic Order via a Laser-Induced Phase Transformation in FeRh Thin Films, Phys. Rev. Lett. **93**, 197403 (2004).

[6] J. Barker and R. W. Chantrell, Higher-order exchange interactions leading to metamagnetism in FeRh, Phys. Rev. B **92**, 094402 (2015).

[7] P. M. Derlet, Landau-Heisenberg Hamiltonian model for FeRh, Phys. Rev. B **85**, 174431 (2012).

[8] J. U. Thiele, S. Maat, and E. E. Fullerton, FeRh/FePt exchange spring films for thermally assisted magnetic recording media, Appl. Phys. Lett. **82**, 2859 (2003).

[9] S. P. Bennett *et al.*, Direct evidence of anomalous interfacial magnetization in metamagnetic Pd doped FeRh thin films, Sci. Rep. **5**, 9142 (2015).

[10] V. D. Buchel'nikov *et al.*, Magnetic shape-memory alloys: phase transitions and functional properties, Phys.-Usp. **49**, 871 (2006).

[11] L. C. Phillips *et al.*, Local electrical control of magnetic order and orientation by ferroelastic domain arrangements just above room temperature, Sci. Rep. **5**, 10026 (2015).

[12] S. Maat, J.-U. Thiele, and E. E. Fullerton, Temperature and field hysteresis of the antiferromagnetic-to-ferromagnetic phase transition in epitaxial FeRh films, Phys. Rev. B **72**, 214432 (2005).

[13] M. Loving *et al.*, Tailoring the FeRh magnetostructural response with Au diffusion, J. Appl. Phys. **112**, 043512 (2012).

[14] L. I. Vinokurova, A. V. Vlasov, and M. Pardavi-Horváth, Pressure effects on magnetic phase transitions in FeRh and FeRhIr alloys, Phys. Status Solidi B **78**, 353 (1976).

[15] T. Naito, I. Suzuki, M. Itoh, and T. Taniyama, Effect of spin polarized current on magnetic phase transition of ordered FeRh wires, J. Appl. Phys. **109**, 07C911 (2011).

[16] R. Barua *et al.*, Tuning the magnetostructural phase transition in FeRh nanocomposites, J. Appl. Phys. **113**, (2013).

[17] X. Marti *et al.*, Room-temperature antiferromagnetic memory resistor, Nature Mater. **13**, 367 (2014).

[18] F. Pressacco *et al.*, Stable room-temperature ferromagnetic phase at the FeRh(100) surface, Sci. Rep. **6**, 22383 (2016).

[19] R. O. Cherifi *et al.*, Electric-field control of magnetic order above room temperature, Nature Mater. **13**, 345 (2014).

[20] T. Goto *et al.*, Growth of FeRh thin films and magnetic properties of FePt/FeRh bilayers, J. Magn. Magn. Mater. **272-276**, E791 (2004).

[21] S. P. Bennett *et al.*, Giant controllable magnetization changes induced by structural phase transitions in a metamagnetic artificial multiferroic, Sci. Rep. **6**, 22708 (2016).

[22] G. C. Han *et al.*, Magnetic stability of ultrathin FeRh films, J. Appl. Phys. **113**, 17C107 (2013).

[23] J. Cao *et al.*, Magnetization behaviors for FeRh single crystal thin films, J. Appl. Phys. **103**, 21 (2008).

[24] C. W. Barton, T. A. Ostler, D. Huskisson, C. J. Kinane, S. J. Haigh, G. Hrkac, and T. Thomson, Substrate induced strain field in FeRh epilayers grown on single crystal MgO (001) substrates, Sci. Rep. (to be published).

[25] J. Kudrnovský, V. Drchal, and I. Turek, Physical properties of FeRh alloys: The antiferromagnetic to ferromagnetic transition, Phys. Rev. B **91**, 014435 (2015).

[26] V. L. Moruzzi and P. M. Marcus, Antiferromagnetic-ferromagnetic transition in FeRh, Phys. Rev. B **46**, 2864 (1992).

[27] J. A. Ricodeau and D. Melville, Model of the antiferromagnetic-ferromagnetic transition in FeRh alloys, J. Phys. F: Met. Phys. **2**, 337 (1972).

[28] L. M. Sandratskii and P Mavropoulos, Magnetic excitations and femtomagnetism of FeRh: A first-principles study, Phys. Rev. B **83**, 174408 (2011).

[29] S. Jekal, S. H. Rhim, S. C. Hong, W.-j. Son, and A. B. Shick, Surface-termination-dependent magnetism and strong perpendicular magnetocrystalline anisotropy of an FeRh(001) thin film, Phys. Rev. B **92**, 064410 (2015).

[30] T. A. Ostler *et al.*, Crystallographically amorphous ferrimagnetic alloys: Comparing a localized atomistic spin model with experiments, Phys. Rev. B **84**, 024407 (2011).

[31] O. N. Mryasov, Magnetic interactions and phase transformations in FeM, M = (Pt,Rh) ordered alloys, Phase Transitions **78**, 197 (2005).

[32] B. Skubic, J. Hellsvik, L. Nordström, and O. Eriksson, A method for atomistic spin dynamics simulations: implementation and examples, J. Phys.: Condens. Matter **20**, 315203 (2008).

[33] T. L. Gilbert, A phenomenological theory of damping in ferromagnetic materials, IEEE Trans. Magn. **40**, 3443 (2004).

[34] W. F. Brown, Thermal fluctuations of a single-domain particle, Phys. Rev. **130**, 1677 (1963).

[35] O. G. Mouritsen, B. Frank, and D. Mukamel, Cubic Ising lattices with four-spin interactions, Phys. Rev. B **27**, 3018 (1983).

[36] E. Mancini *et al.*, Magnetic phase transition in iron–rhodium thin films probed by ferromagnetic resonance, J. Phys. D: Appl. Phys. **46**, 245302 (2013).

[37] Z. Q. Liu *et al.*, Full Electroresistance Modulation in a Mixed-Phase Metallic Alloy, Phys. Rev. Lett. **116**, 097203 (2016).

[38] S. B. Roy, P. Chaddah, V. K. Pecharsky, and K. A. Gschneidner, Overview No. 145 Metamagnetic transitions, phase coexistence and metastability in functional magnetic materials, Acta Mater. **56**, 5895 (2008).